Airborne C-band RFI Measurements with PSR/CXI and CISR from the WB-57 aircraft: Initial Data Examination

J. T. Johnson*, B. Guner, N. Niamsuwan, and M. Valerio

March 13, 2006

Contents

*The Ohio State University, ElectroScience Laboratory, 1320 Kinnear Road, Columbus, OH 43210, USA. Email: johnson.1374@osu.edu

1 Introduction

This report provides initial documentation of observations of C-band RFI made from NASA's WB-57 high-altitude aircraft using the PSR/CXI system of NOAA/ETL and the C-band Interference Suppressing Radiometer (CISR) [1] digital backend of the Ohio State University (OSU) ElectroScience Laboratory. The C-band Agile Digital Detector (CADD) system of the University of Michigan [2] was also included in the campaign; results from that system will be reported elsewhere. The observations described in this report were performed during a test flight on Aug. 25th, 2005 beginning at Ellington Field, Houston, TX and including overflights of Dallas and San Antonio as well as a flight segment over the Gulf of Mexico. Only data for which both CISR and PSR/CXI information was available are discussed here, in particular only the vertically polarized C-band measurements. The PSR/CXI instrument also recorded horizontally polarized and polarimetric C-band channels, as well as X-band brightnesses in multiple frequency sub-bands, but these were not sampled by CISR during the flight.

2 Instrumentation

2.1 PSR/CXI

Reference [1] provides a description of the combined PSR/CXI and CISR system; here the relevant information is briefly reviewed. The PSR/CX instrument of NOAA/ETL has been deployed in several previous airborne remote sensing campaigns [3], and provides well calibrated brightness measurements along with a variety of possible scanning patterns during flight operations. The majority of the data to be presented were obtained from conically scanned observations (i.e. the antenna is rotated in azimuth at a fixed speed) at a fixed incidence angle of 55 degrees from nadir (when in level flight). One portion of the dataset near the end of the flight includes fixed scan angle sky observations during steep rolls of the aircraft for calibration verification purposes. The antenna 3 dB beamwidth (two-sided) is approximately 10 degrees for all observations.

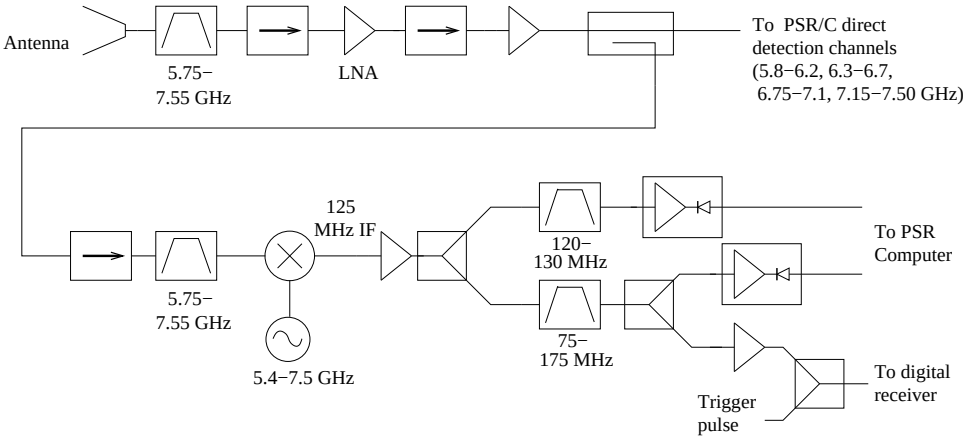

Figure 1: Simplified schematic of PSR/CXI

The PSR/CX instrument includes four C-band sub-channels, with respective 3 dB bandpass frequency ranges of 5.8-6.2, 6.3-6.7, 6.75-7.1, and 7.15-7.5 GHz. These sub-channels can provide some measure of RFI mitigation, but remain large analog channels ($\sim$400 MHz) compared to the bandwidth of likely RFI sources. The PSR/CXI instrument utilized in this flight is a modification of PSR/CX that includes a downconverter module so that tuned observations can be made throughout C-band in a narrower bandwidth than the 400 MHz of the main channels. Figure 1 is a simplified schematic of the PSR/CXI, and shows that following initial filtering and front-end amplification, a portion of the antenna power is coupled to the downconverter section. The local oscillator (LO) utilized is capable of tuning from 5.4 to 7.5 GHz, uses a 125 MHz IF center frequency, and provides $>$ 20 dB rejection of the upper RF side band. The IF signal is filtered to both 10 and 100 MHz bandwidths, and both of these bandwidths are passed through a logarithmic amplifier/detector, power integrated, and recorded. The 100 MHz bandwidth signal is also passed through a linear amplifier; a portion of this coherent signal is coupled to the CISR instrument in the cabin rack of the P-3, while the remainder is detected, power integrated, and recorded by PSR/CXI (PSR/CXI post-amplifier section not shown in Figure 1). Tuned channel observations recorded by the PSR are reported elsewhere [4], and are not considered further here.

For the CISR data to be reported, the LO was tuned so that 100 MHz channel observations were made at 5.5-5.6, 5.6-5.7, ..., 7.6-7.7 GHz; this is a set of 22 channels. The LO was swept continuously throughout the flight, with each channel being observed for approximately 37 msec; a complete sweep of channels required approximately 814 msec. The PSR/CXI LO is a YiG-tuned device [5], and therefore is subject to hysteresis effects as well as temperature sensitivity. For this reason, the accuracy of the RFI frequencies should be taken as $\approx \pm 2$ MHz throughout this report. Although this is acceptable accuracy for radiometric studies, possible inclusion of an LO with improved tuning accuracy and stability deserves consideration for future flights of PSR/CXI.

2.2 CISR

A simplified schematic of the CISR instrument is provided in Figure 2. The CISR digital receiver backend measures the incoming 100 MHz bandwidth through the use of two 200 MSPS A/D converters, each of which samples the band 125-175 MHz. A "channel-selection" is therefore required to upconvert the 75-125 MHz portion of the PSR/CXI IF signal to 125-175 MHz. Following A/D conversion, the CISR instrument can perform an "asynchronous pulse-blanking" (APB) [6] operation to suppress temporally localized interference, as well as a 1024 point FFT operation, followed by optional power integration or max-hold computations. Using the notation of [1], the following digital receiver modes were utilized in the August 25th, 2005 test flight:

- Mode 0: Integration, APB off
- Mode 4: Capture

In Mode 0, the 1024 point FFT operation is performed, followed by power computation and an integration over a 1.3 msec time period. The output in this mode is then a spectrum of the power in 1024 $\sim$100 kHz bandwidth sub-channels within the tuned 100 MHz spectrometer channel. This fine spectral resolution can provide improved capabilities for identifying and suppressing frequency-localized interference. The Mode

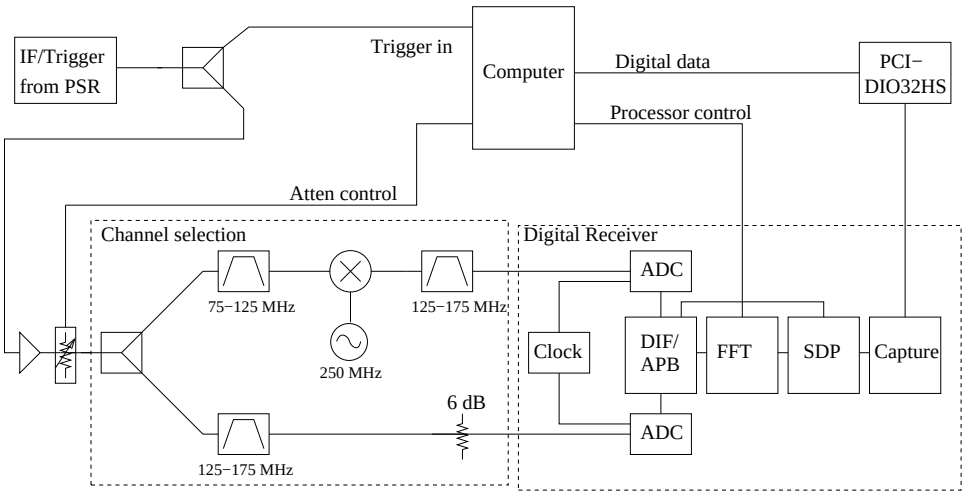

Figure 2: Simplified schematic of CISR

4 "capture" mode refers to direct recording of the sampled 100 MHz channel at 10 nsec temporal resolution with no further processing.

CISR's asynchronous pulse blanking (APB) algorithm was not used in this campaign due to the relative infrequency of pulsed interferers at C-band, as well as a desire to optimize calibration of the Mode 0 data. Previous L-band experiments [7] have clearly demonstrated the effectiveness of the APB algorithm at mitigating pulsed source interference while maintaining accurate brightness temperature measurements.

2.3 Interface Between PSR/CXI and CISR

Because it is the PSR/CXI data acquisition computer that controls oscillator tuning in the downconverter, the CISR and PSR/CXI computers must be interfaced. To make this interface as simple as possible, a simple 1-bit "trigger" signal was used. This TTL-level pulse is sent from the PSR/CXI control computer to the CISR computer whenever a tuning operation has been completed and measurements should begin. In addition, both computers include highly accurate on-board clocks, synchronized through the IRIG-B standard, so that knowledge of the oscillator frequency for a particular CISR measurement is obtainable by matching up recorded trigger pulse times in post-processing of a joint data set. In the data considered here, unambiguous matchups of the PSR/CXI and CISR measurements were possible utilizing this

process. Offsets in the two "timestamps" were within 3 msec for the majority of the recorded data.

One issue in this time synchronization involves observations of the internal noise diodes of the PSR/CXI system. These noise diodes are useful for verifying or improving system calibration stability between measurements of the external hot and cold targets embedded in the PSR/CXI scanhead. The simple 1-bit trigger interface however does not allow specification of the noise diode switch state during a measurement. To address this issue, a plan was developed wherein the noise diode measurements were to be performed within a specified time interval following the trigger signal. However, the time accuracy of the PSR/CXI instrument states was insufficient to ensure an accurate noise diode measurement by CISR at each opportunity. It is recommended that future work address this issue by providing more precise control of PSR/CXI instrument state timing, or by implementing a trigger signal with two or more distinct voltage levels, so that a unique trigger for the noise diode measurements can be provided.

2.4 CISR modifications for the WB-57 aircraft

A few modifications to the CISR hardware from the implementation reported in [1] were performed, primarily to improve survivability in the high altitude environment. The CISR hardware was located in a unpressurized portion of the WB-57 aircraft, and therefore exposed to the ambient (though inside the aircraft) air temperature and pressure at altitude. Figure 3 is a photograph of the CISR enclosure when installed within the "foreward racks" in the WB-57 aircraft.

2.4.1 Atmospheric pressure issues

The low atmospheric pressure of approximately 0.1 atm at altitude (62500 ft) complicates heat dissipation issues within the CISR enclosure, and also requires use of modified hard drive systems for recording observed data. Though solid state hard drives are desirable in such cases, the high data rate of CISR makes use of faster magnetic drives preferable. In this campaign, the CISR operating system and source

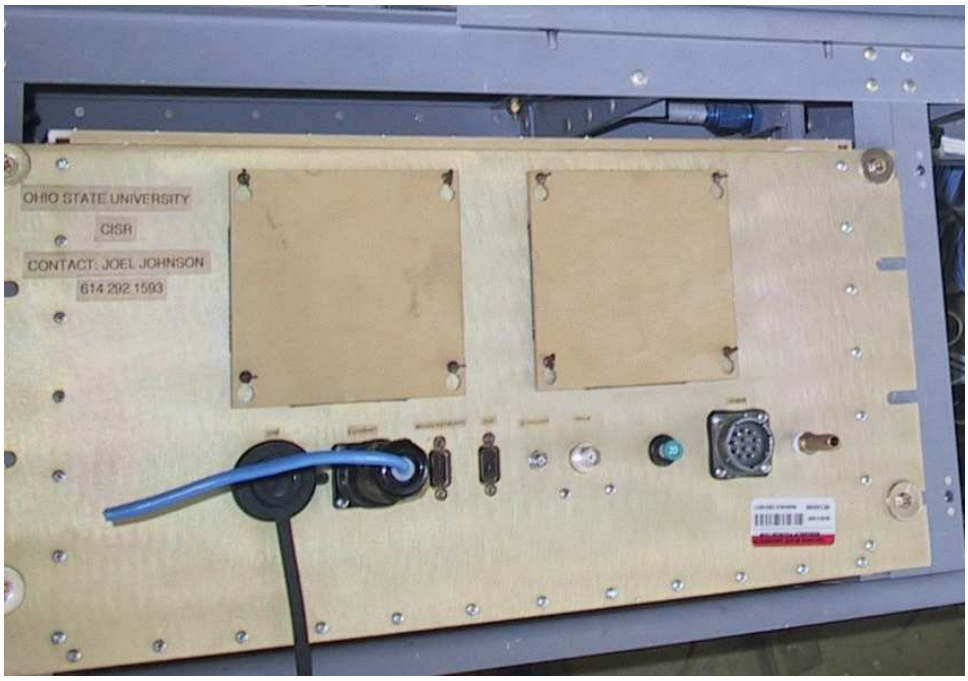

Figure 3: Photograph of the CISR enclosure installed on the WB-57 aircraft

executable were placed on a 4 GB solid state drive, while data was stored on an 80 GB sealed magnetic hard drive. In an earlier deployment of CISR on-board the WB-57 aircraft (April 2005), the latter drives failed due to improper sealing by the vendor. However these problems were corrected by the vendor prior to August 2005, and no further issues were encountered.

2.4.2 Temperature control

CISR was further modified to include simple temperature control systems. A set of heaters capable of providing 175 W of heating were included, under the control of a thermostat within the CISR enclosure which turned the heaters on when the temperature of the thermostat declined below 10 C. A second thermostat was also included at an alternate location within the enclosure to override the heater on state if temperatures greater than 50 C were encountered at a second thermostat. Thermostats were also placed within the enclosure to turn CISR electronics off when the internal temperature decreased below 0 C or above 50 C. These thermostats were simple on/off bimetal thermostats, and their status was not monitored or recorded.

The CISR enclosure included substantial thermal insulation due to the low ambient air temperature at altitude. Given this insulation and the existing heating provided by the CISR electronics, it is not believed that the heating system was utilized during flight.

The reduced amount of convective cooling available at low atmospheric pressure increases the possibility of localized "hot-spots" within the CISR enclosure, even though many portions of the enclosure may be cold. The only enclosure temperature information recorded during the flight was obtained from a temperature, humidity, and pressure monitoring card within the CISR PC-104 computer. Data from this sensor indicated local temperatures approaching but not exceeding 62 C. While further consideration of CISR thermal transfer could possibly reduce the likelihood of these high internal temperatures, rated operational temperatures for CISR electronic components exceed 62 C, and no apparent problems were observed.

2.4.3 Condensation

A final modification was made in an attempt to reduce the amount of condensation within the CISR enclosure as the aircraft returns from altitude. Though the enclosure was not hermetically sealed, and in fact becomes an explosive hazard if pressurized relative to the ambient environment, attempts were made to keep the enclosure reasonably air tight with the exception of a single air exchange opening. This opening was routed through a tube desiccator, so that air taken into the enclosure upon descent would contain a reduced moisture content. The PSR and University of Michigan systems utilized a similar approach to reduce condensation problems. Though quantitative information on the performance of this system was not recorded, no damage due to condensation within the CISR enclosure was encountered.

2.5 Measurement Process

2.5.1 PSR Observation and Spot Properties

As stated previously, the PSR/CXI LO was continuously tuned through the 22 bands of interest throughout flight operations, requiring approximately 814 msec to complete

a sweep. When in conical scan mode, the PSR/CXI antenna rotation period was typically 40 seconds, so that 49.1 sweeps were performed per antenna "scan" (i.e. rotation). PSR conical scan mode observations were performed in a total of 137 antenna rotations during the flight.

At the typical flight altitude of 62500 ft, and using the nominal PSR antenna 3 dB beamwidth (two-sided) of 10 degrees, the 3 dB footprint observed by the antenna is approximately 10.3 km in diameter along track. At the typical flight speed of 205 m/sec, the 40 sec scan rate results in an along track sampling distance of 8.2 km, slightly less than the 3 dB footprint size. The cross-track 3 dB footprint is approximately 4.75 km in diameter; this dimension represents approximately 1/36 of the circumference of the cross-track scan. Therefore each independent cross-track footprint is observed for more than a second during the scanning process, allowing more than a full sweep of the 22 tuned channels within each footprint.

As the PSR antenna rotates these 4.75 km by 10.3 km spots are swept in a circle along the Earth surface of approximate diameter 64.3 km (between 3 dB spot boundaries.) Thus, data from one PSR rotation represents observations comparable in spatial dimensions to a typical C-band satellite footprint, although the total area observed is only approximately half of the complete 64.3 km diameter circle. Based on these properties, it appear reasonable to assume that RFI effects in single pixel satellite observations are roughly comparable to those observed in a complete PSR antenna rotation.

2.5.2 CISR Operational Process

CISR was configured to observe in "average, APB off" mode for 16 consecutive sweeps of the tuned channels (around 13 seconds), followed by "capture" mode observations for 2 consecutive sweeps (around 1.63 seconds). CISR then paused for approximately 4.6 seconds to write the recorded data to its internal hard drives. This results in an approximate 19 second periodic pattern, completed approximately twice per PSR antenna rotation. In "average, APB off" mode, a base temporal resolution of 1.3 msec was utilized, with 12 1024 point spectra obtained in 15.75 msec following each

PSR/CXI trigger. In the capture mode, a 128K capture (1.3 msec) was recorded for each PSR/CXI trigger. The resulting CISR data rate is approximately 9.2 GB/hr; although this is certainly unacceptable for end-user radiometer applications, the goal of recording as much information on the observed RFI as possible results in the high data rate for this study.

2.5.3 Calibration

The PSR main channel data to be reported was "quick-calibrated" using the external hot and cold loads of the PSR scan head; this procedure is expected to produce brightnesses typically accurate to within 1-2 K for the obtained 20 msec observations. The PSR "VIEWRAD" processing system was utilized for this purpose, as well as for forming scan images of measured brightnesses. Cal load observations were performed following 8 rotations of the PSR antenna for the majority of the flight. Examination of the PSR main channel data following calibration showed the expected 1-2 K standard deviations for PSR main channels 2 through 4, but an increased standard deviation of around 4 K in PSR main channel 1. This appears to have resulted due to a decreased system gain in main channel 1. However it is possible to reduce these standard deviations further by performing an additional integration over scan angle. This is because the standard PSR observation occurs every 37 msec, which represents only 0.33 degrees of scan angle, compared to the 3 dB spot of 10 degrees. PSR scan angle images to be illustrated have therefore undergone an additional smoothing by taking an average over the 9 surrounding pixels; this reduces the standard deviation by a factor of 3. The low gain of channel one also reduces the accuracy of its absolute calibration relative to the other channels. This offset among channels plays a role in decreasing the sensitivity that can be achieved by the PSR four channel RFI mitigation algorithm.

Calibration of the tuned PSR/CXI and CISR channels is also available through this process, and the slower scan rate and corresponding increased cal load observation time result in greatly improved CISR calibration compared to [1]. However, as with PSR main channel 1, calibration of CISR data below 6.2 GHz remains problematic

due to the low apparent gain of the PSR front end in this region. For this reason, many of the plots to be shown will be presented in terms of relative power variations in raw data, although calibrated data will also be illustrated for CISR channels above 6.2 GHz. No additional scan angle integration of these data are performed due to the tuning process. Note that some evidence of corruption of the PSR main channel calibration procedure due to strong RFI during cal-target observations is observed in the campaign, although the majority of the cal-load observations appear to be RFI-free.

3 Experiment Conditions

Table one provides information on the flight plan. Figure 4 illustrates the geographical region observed; note major cities including Houston, Dallas-Fort Worth (DFW), and San Antonio, are marked with circles. Figure 5 is a plot of the WB-57 altitude versus time. As can be determined from Table 1, the flight plan included takeoff from Ellington Field (Houston area) at 17:14 along a West-Northwesterly heading, followed by a turn to the North near Krebsville (a small town) at 17:32. Ascent to a flight altitude near 62000 ft was completed by 17:51 as the DFW area was approached. The flight path then included a turn to the South over DFW around 18:00, followed by observations over more rural Texas locations until an overflight of San Antonio around 18:30. A turn to the Southeast over San Antonio then led to an overflight of the Gulf of Mexico beginning at 18:49. The flight plan then included a short circular flight at roll angle 30 degrees beginning at 18:54, followed by steeper rolls to allow sky observations beginning at 18:59. These rolls were completed by 19:06, and all observations stopped at 19:11. The aircraft returned to Ellington field at 19:42.

PSR and CISR were both powered on before takeoff, and both acquired data until 19:11. However the analysis reported here focuses on conically scanned data obtained after flight altitude was reached (17:51) and before the circle flights were begun (18:54). The ADD system was powered on after reaching altitude 25,000 ft (17:23) and observed until all systems were powered off at 19:11. The dataset contains observations in a variety of RFI environments, including urban, rural, and

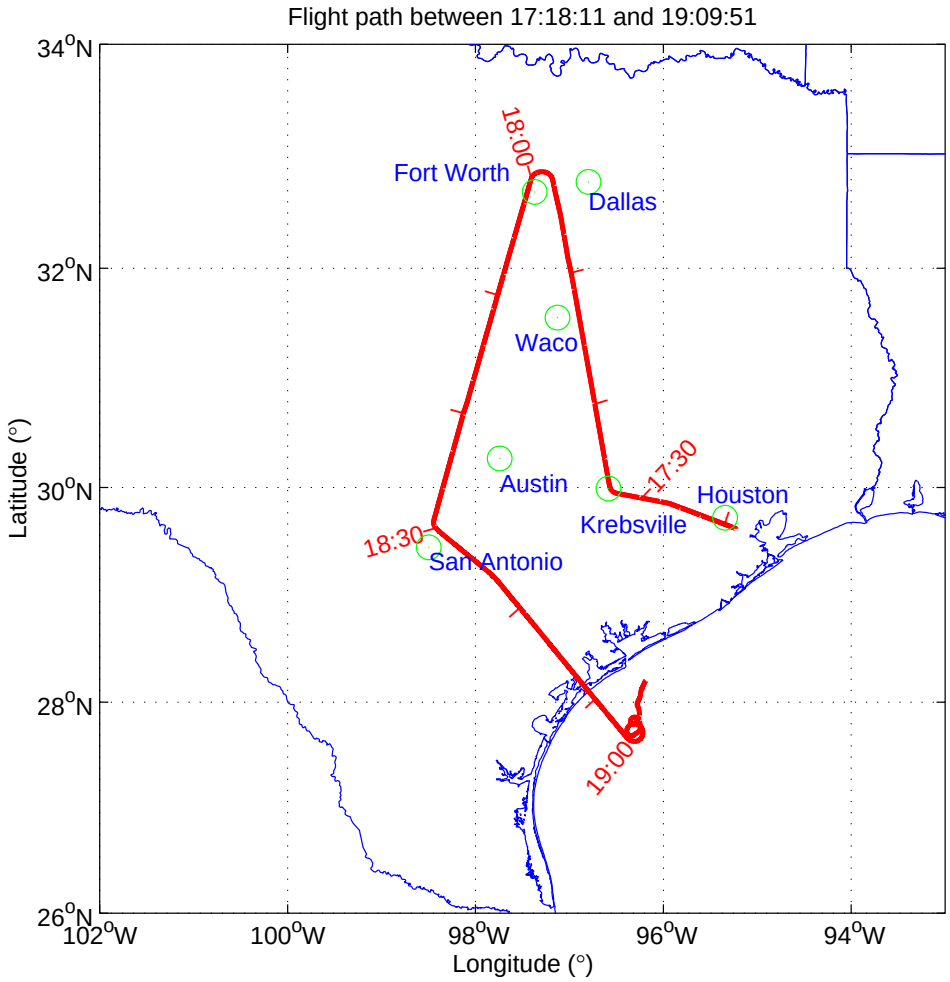

Figure 4: Flight path, including nearby Texas cities (circles)

Time (UTC)	Event	Comments
17:14	Takeoff from Ellington Field	
17:17	Start PSR conical scans	
17:23	Altitude 25 kft, ADD on	Depart Houston vicinity
17:32	Turn Northward over Krebsville	Heading 280 degrees to 354 degrees
17:51	Altitude 62 kft	Approaching DFW
17:59	Over DFW	Turn toward San Antonio
18:30	Over San Antonio	Turn toward coast
18:49	Over Gulf of Mexico	
18:52	Begin descent from flight altitude	
18:54	Begin circle flight	roll 30 deg
18:59	Stop PSR conical scans	Short rolls up to 60 deg
19:06	Finish cal rolls	
19:11	PSR off	
19:42	Land at Ellington Field	

Table 1: Time history of flight on August 25th, 2005

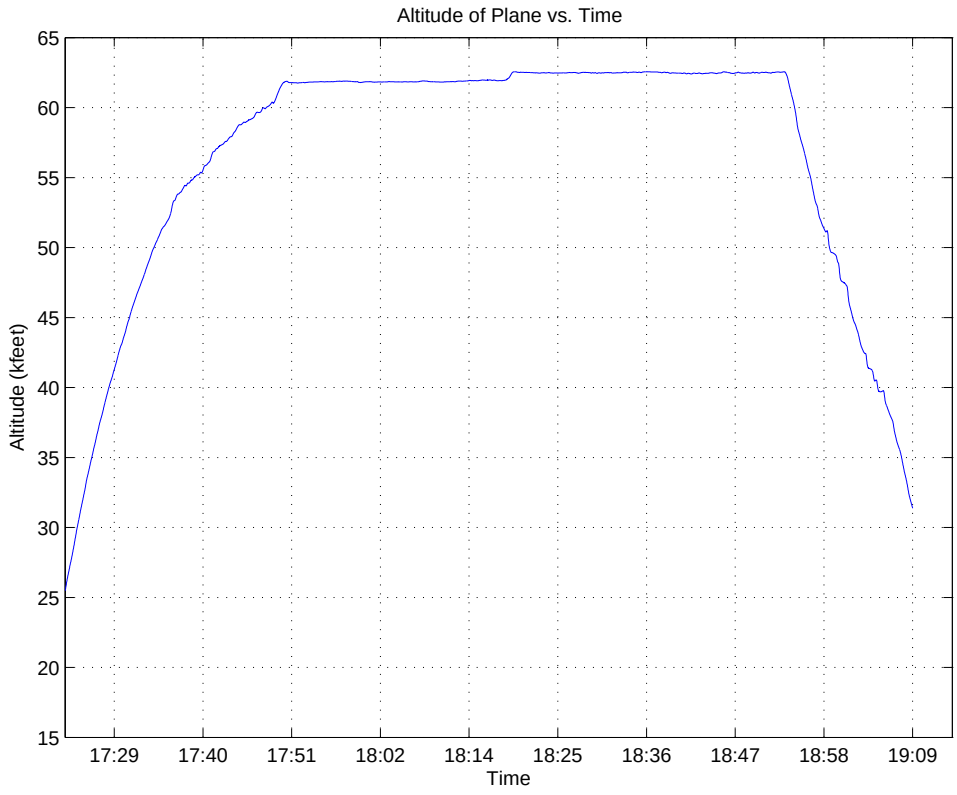

Figure 5: Altitude of WB-57 aircraft versus time

water scenes. Although detailed geo-location of the measured data can be performed, for simplicity the images of PSR/CXI conically scanned data to be shown will be presented in terms of time and scan angle; these should not be taken as geographic images given possible variations in the aircraft heading, pitch, roll, and altitude.

RFI source information from the JSC database

A review [8] of the NPOESS RFI source database obtained from the Joint Spectrum Center (JSC) [9] was performed to assist in preliminary interpretation of the datasets to be described in the next sections. The JSC database utilized contains data not updated since 1999, and therefore is subject to significant errors as well as source omissions. Within the frequency ranges of interest, the JSC database is described as including only 5.5-5.9 GHz and 6.2-7 GHz, and the database also omits classified source information. Nevertheless, it is this dataset that has been utilized by the IPO in performing RFI simulation studies, so that information on the accuracy of this particular database is relevant. The dataset also provides some degree of information on the spatial distribution of RFI sources.

Figure 6 plots RFI source locations in the frequency range of interest taken from apparently valid records in the JSC database. The flight path is indicated by the thick red line, and the Houston, DFW, and San Antonio areas are marked by the large circles. The strong correlation of the source density with urban locations is clear. The portion of the flight encountering the smallest source density is found between the DFW and San Antonio areas. Note that some off-coast sources are also included in the database.

A histogram of center frequencies for the sources included in Figure 6 is provided in Figure 7. Overall the distribution is fairly uniform from 6.2-7 GHz, with the exception of the region 6.4-6.6 GHz, which contains a smaller number of sources. Note again that sources centered from 5.9-6.2 GHz are described as "not included" in the database, so that the histogram should not be taken as accurate in this region. Database information also reveals that many of the allocations below 5.9 GHz are

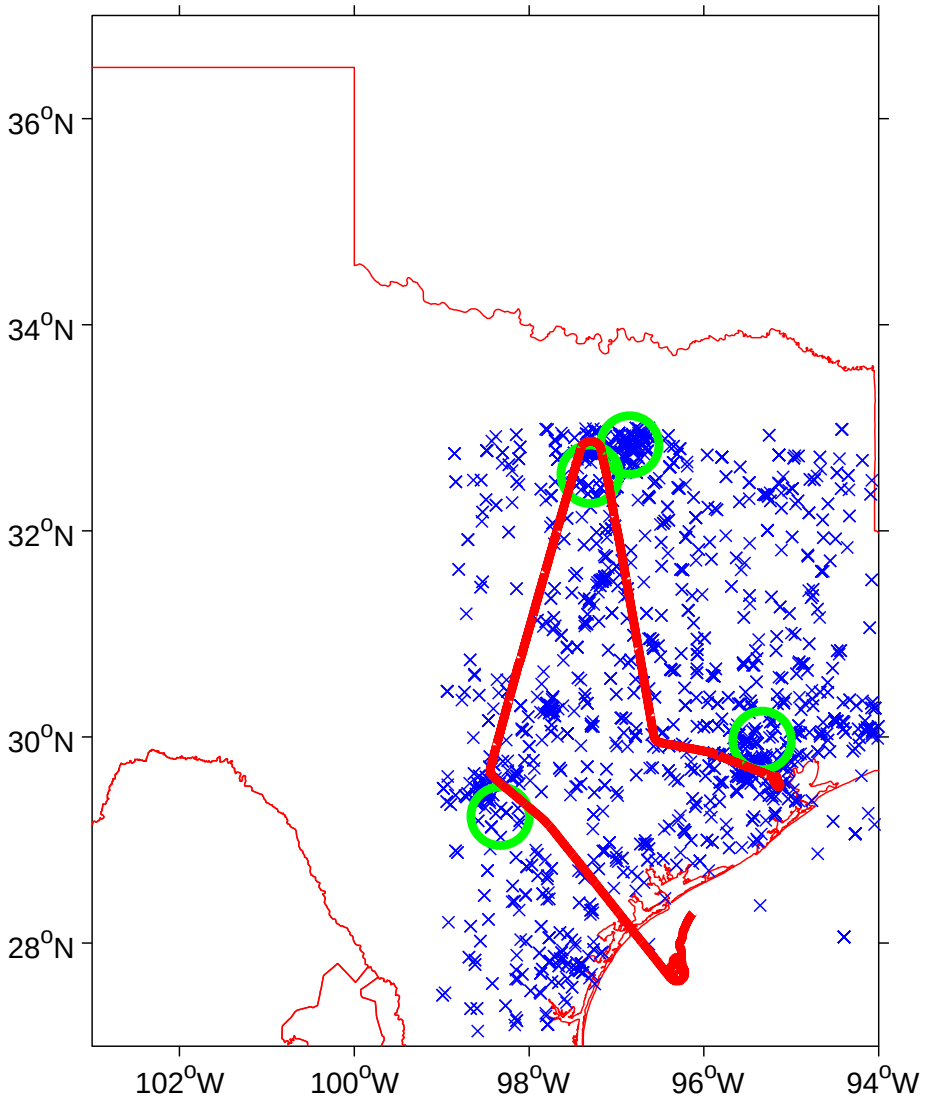

Figure 6: Locations of C-band RFI sources within the JSC source database. Flight path is indicated by the thick red line.

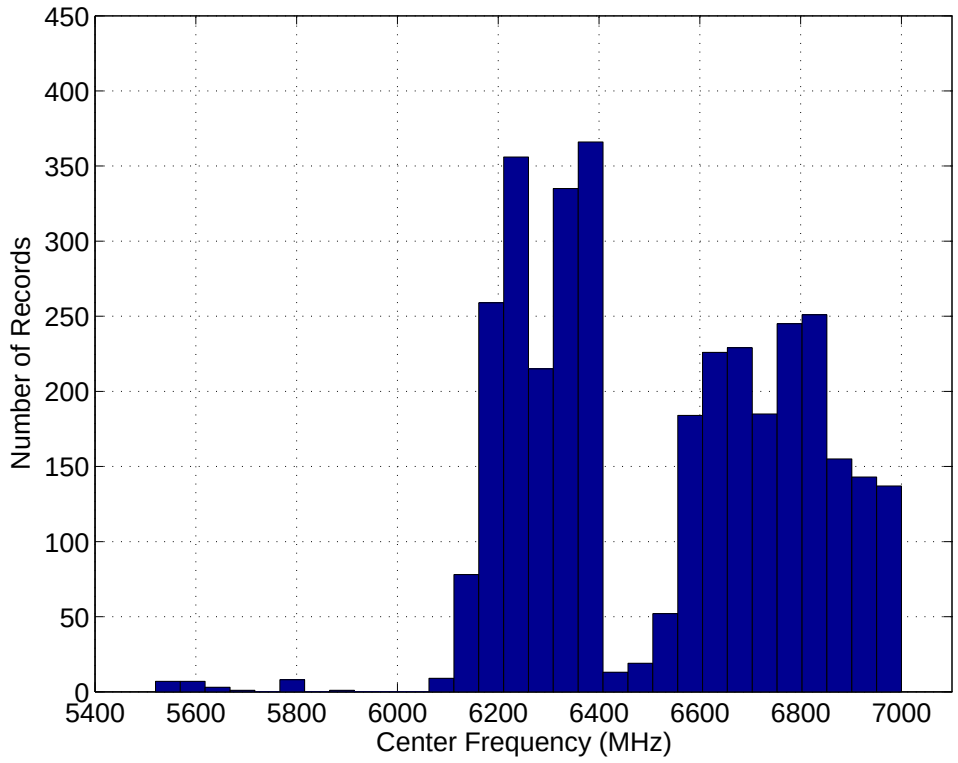

Figure 7: Distribution of source center frequencies for the JSC database records plotted in Figure 6. Note that records centered between 5.9-6.2 GHz are described as "not included" in the database.

associated with radar or other pulsed sources, while those above 5.9 GHz are primarily communication systems.

4 PSR scan images

Figure 8 plots PSR scan angle images for the foreward part of the PSR conical scan, in all four PSR "main" channels. Obvious RFI is common in these images, with brightnesses up to 10700 K, 2994 K, 2442 K, and 2660 K observed in channels one through four, respectively. Of these channels, channel 1 generally shows the largest degree of RFI corruption, and channel 4 the least, although obvious RFI remains present in channel 4. Increase RFI associated with the Houston (prior to 17:25), DFW (around 18:00), and San Antonio (18:30) portions of the flight is apparent. The decreased brightness associated with observations over the Gulf of Mexico is also obvious in the later portions of the images. Figure 9 plots the average of the images

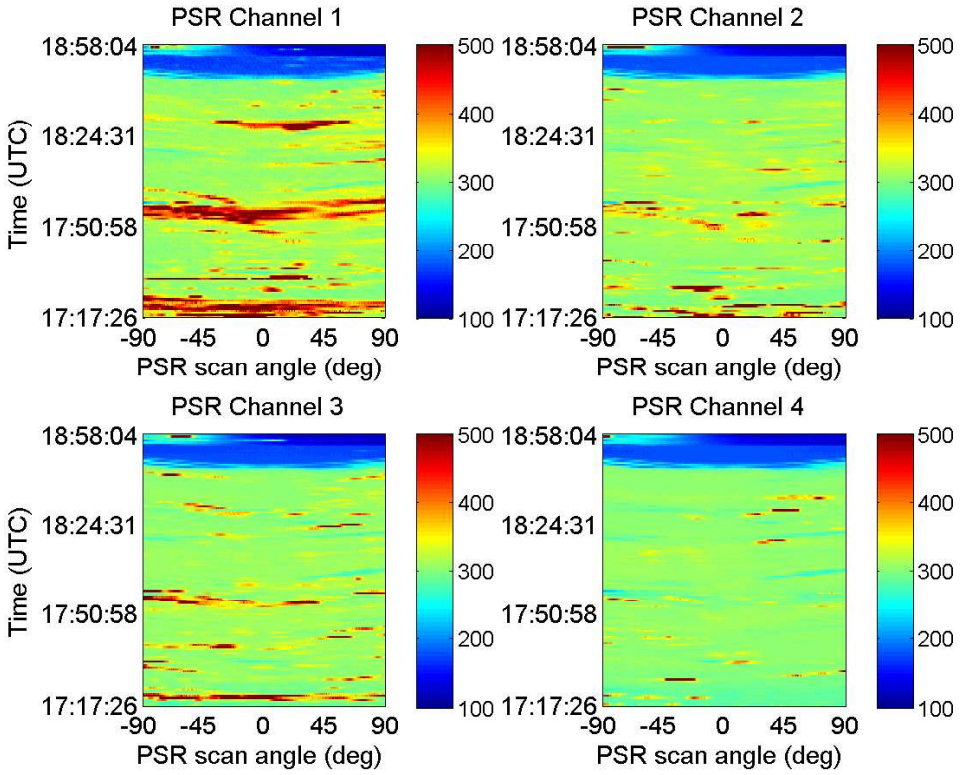

Figure 8: Calibrated brightnesses from PSR conical scans of the entire flight, in all four PSR main channels

in Figure 8 over scan angle, and shows behaviors consistent with those discussed for Figure 8.

As described in [1], it is possible to apply the PSR four sub-channel RFI mitigation algorithm to these images in order to remove RFI corruption. Use of the algorithm in this case eliminates the vast majority of the obvious RFI. However it is difficult to determine the amount of low-level RFI remaining following this processing. A particular problem results when the algorithm determines that three or more channels contain RFI, so that the validity of the remaining channel is difficult to determine. Tables 2 and 3 provide summary statistics from the PSR RFI mitigation algorithm for the time periods 18:08-18:23 (more rural locations) and 17:54-18:08 (near DFW). Statistics are provided in terms of the percent of 21600 pixels determined to have a specified "interference level". A "clean" classification results for a channel only if it is determined to be RFI free and RFI was detected in less than 3 of the remaining channels. The classifications "1 channel" and "2 channel" for a particular channel

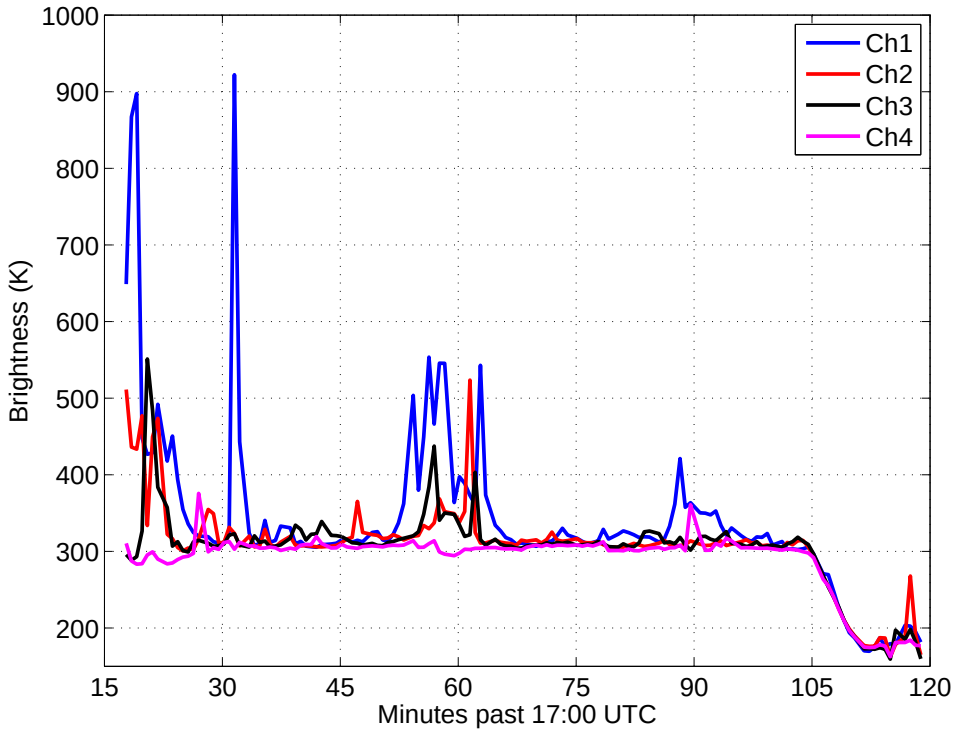

Figure 9: Average of Figure 8 over scan angle, versus time

indicate that that channel was determine to contain RFI when only one or two of the four PSR channels were deemed corrupted. Cases with "3 channels" however result in a classification for all PSR channels, due to the limitations of the algorithm with regard to assessing the remaining channel in this case.

While the percentages shown are influenced by PSR calibration issues and by the particular algorithmic parameters utilized, overall the results clearly indicate a significant RFI problem both in the DFW (53.1% classified as "3 channel") and rural

PSR freq (GHz)	5.8-6.2	6.3-6.7	6.75-7.1	7.15-7.5
Clean %	39.6	41.8	49.1	65.2
1 Channel %	13.0	11.4	3.0	0.6
2 Channel %	19.3	18.8	19.7	5.9
3 Channel %	27.0	27.0	27.0	27.0
Algorithm failed %	1.3	1.3	1.3	1.3

Table 2: Statistics from PSR four sub-band interference suppression algorithm: 21600 pixels over rural Texas (18:08-18:23 UTC)

PSR freq (GHz)	5.8-6.2	6.3-6.7	6.75-7.1	7.15-7.5
Clean %	12.5	30.8	30.6	44.1
1 Channel %	10.7	3.6	1.5	0.1
2 Channel %	22.6	11.5	13.8	1.7
3 Channel %	53.1	53.1	53.1	53.1
Algorithm failed %	1.1	1.1	1.1	1.1

Table 3: Statistics from PSR four sub-band interference suppression algorithm: 21600 pixels near DFW (17:54-18:08 UTC)

(27.0% percent "3 channel') observations. Other statistics show a decreased, but non-negligible, presence of RFI in the highest frequency PSR channel, consistent with the scan images of Figure 8.

Examination of CISR data can be used to help to reveal further the properties of the RFI encountered, its distribution in frequency, and its temporal properties; examples of these analyses are presented in the next section. To simplify the discussion, CISR data will be compared with PSR scan plots from three individual PSR antenna scans: one over DFW (scan 57), one in rural Texas (scan 72), and one over the Gulf of Mexico (scan 129). These scans represent 40 seconds of PSR data, during which CISR operated in "average, APB off" mode for approximately 26 seconds and in "capture" mode for approximately 3.2 seconds.

5 CISR observations near DFW

Observations from 17:59:09 to 17:59:49 (a complete PSR antenna rotation) were selected as a representative dataset observed near Dallas-Fort Worth. Figure 10 is a plot of the PSR main channel brightnesses versus time; a high degree of RFI corruption is observed, with brightnesses in channels one through three frequently exceeding 350 K. Channel four shows less evidence of RFI, but obvious RFI corruption is observed in two locations, where brightnesses approach 360 and 380 K, respectively. For this scan, the PSR algorithm classifies 67% of pixels as containing RFI in 3 or more channels.

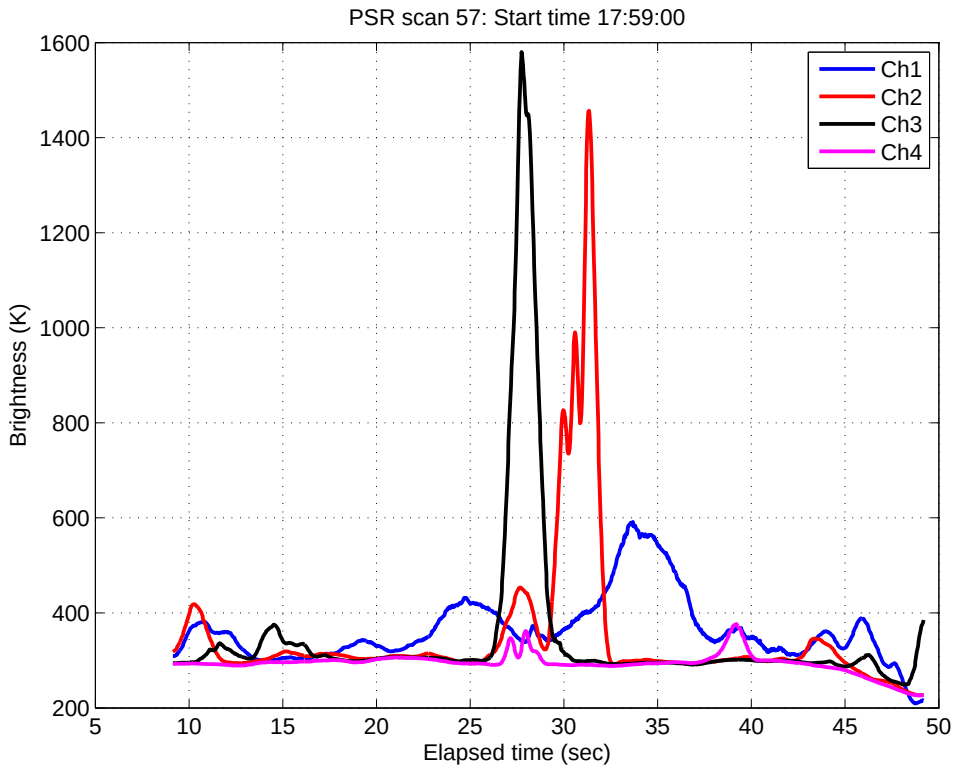

Figure 10: Vertically polarized brightnesses versus time for four PSR main channels during a portion of the flight over the Dallas-Fort Worth area

Time histories of selected CISR channels in "average, APB off" mode during this portion of the flight are illustrated in Figures 11 and 12. The figures represent relative power variations in the 1024 CISR sub-channels within a given 100 MHz tuned PSR channel, versus sample number. These sample numbers increase with time, but are not necessarily contiguous due to changes in the CISR observational mode as well as CISR's pausing to write data to the hard drive. For this reason, formation of scan angle images from these data result in gaps in the scan angle coverage, so that the plot format used in Figures 11 and 12 is preferable. Determination of the exact time of a particular CISR observation remains possible if desired. Channels omitted from Figures 11 and 12 did not contain obvious RFI on the scales of the plots illustrated.

The colorscale of the images represents the relative power variations of the observed data relative to the mean CISR power in a given sub-channel. These relative power variations are converted to decibels, so that 0 dB indicates a constant power level, while increases of 1 or more dB indicate significant interference. Note that CISR images near the center of each channel (50 MHz from the left hand side of each plot) do not contain reliable data due to reduced CISR gain in the cross-over between the two CISR ADC channels.

Figures 11 and 12 clearly contain a wide variety of source emissions, ranging from extremely wideband (the source apparently centered near 5.8 GHz in Channels 3-4 with an apparent bandwidth on the order of 70-80 MHz), down to extremely narrowband sources (examples in Channel 1, 2, 8, 11, 13, 14, 16, 19, and 22, among others.) Many of the C-band communications system allocations of the FCC allow bandwidths up to 30 MHz; several of these systems are apparent particularly in Channels 8 and 11. Overall this scan clearly indicates the significant number of RFI sources that are encountered in major urban areas within the United States.

Figure 13 illustrates the mean and maximum CISR calibrated brightnesses observed in Figures 11 and 12 versus frequency for CISR channels greater than 6.2 GHz. Both the mean and maximum plots show evidence of RFI, although the maximum plot is much more sensitive to RFI occurring in only a portion of the images in Figures 11 and 12. RFI brightnesses exceeding 10,000 K are frequently observed, par-

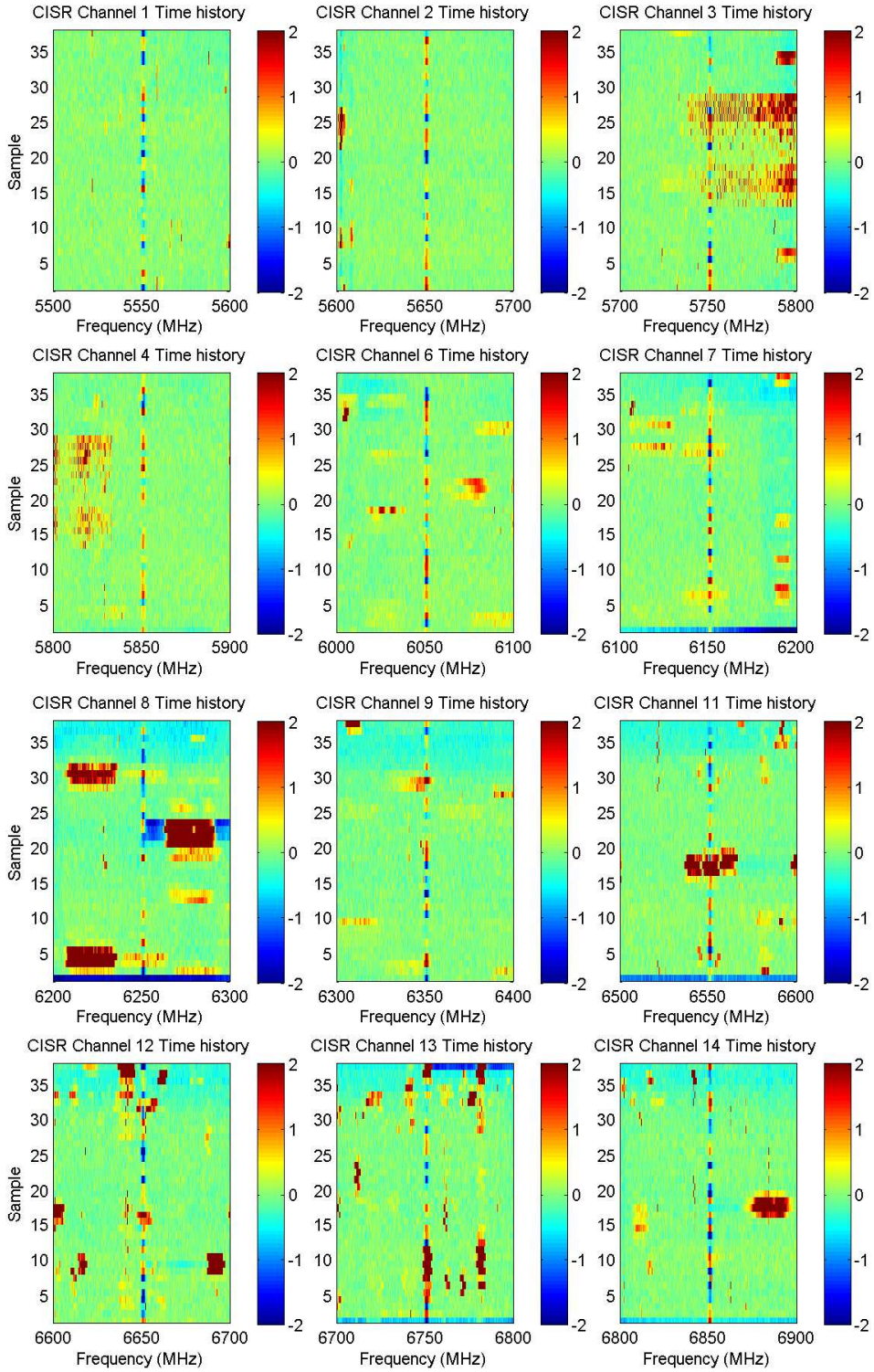

Figure 11: Time histories of selected CISR normalized spectra for portion of flight shown in Figure 10

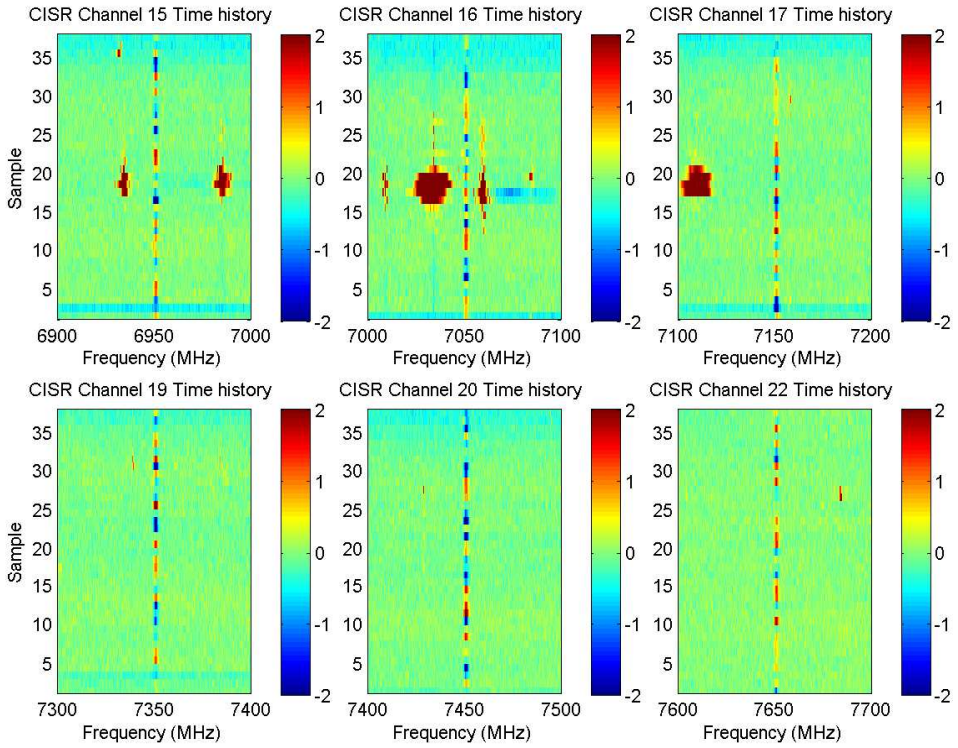

Figure 12: Time histories of selected CISR normalized spectra for portion of flight shown in Figure 10

ticularly in the ranges 6.2 to 6.4 GHz and 6.5 to 7.1 GHz. CISR observed maximum brightnesses exceed those of the PSR main channels because CISR is able to resolve RFI source emissions in frequency, whereas the PSR main channels average these contributions over frequency. Figure 13 also includes vertical lines marking the 3 dB (dashed black) and 40 dB (green) boundaries of the four proposed CMIS channels. These channels are 190 MHz each in bandwidth; the information on these channels used was current as of Sept 2005 [10]. Results show strong RFI in all of the proposed CMIS channels, although RFI in CMIS channel 4 is reduced compared to the other CMIS channels.

More detailed analysis of this dataset is available through an interactive data analysis tool (IDAT) (based in Matlab); this tool allows matchups of CISR and PSR data to be examined while providing geolocation and other information. Further studies will attempt to match the sources observed in this overpass with licensed sources from the FCC as well as the JSC database; the FCC's license locator tool can be used for

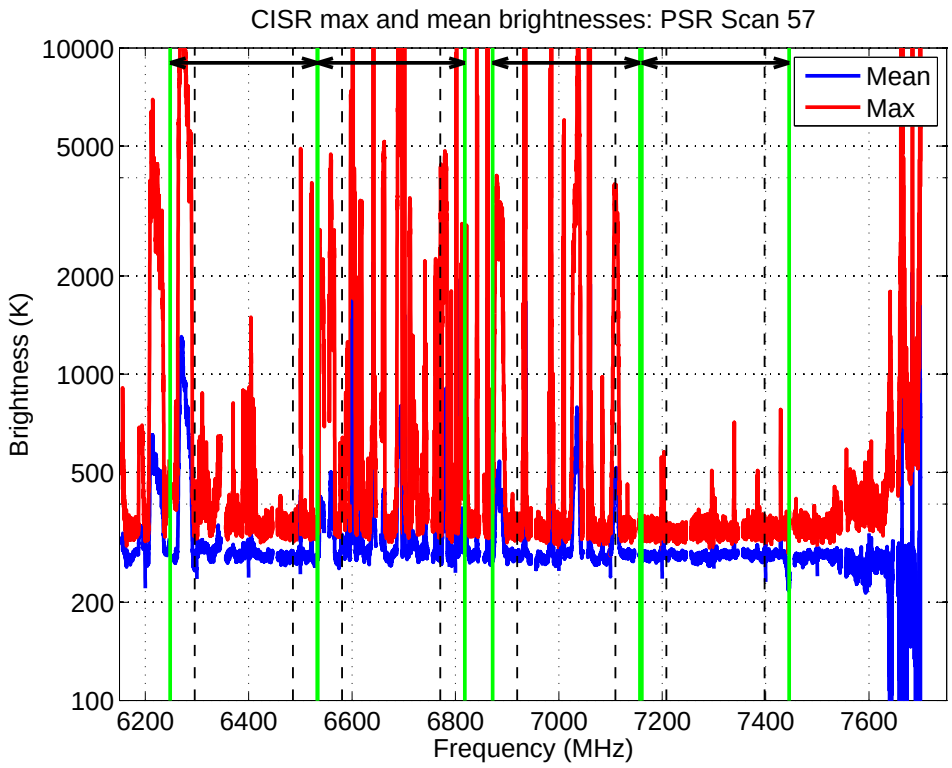

Figure 13: Mean and maximum CISR brightnesses observed in Figures 11 and 12 versus frequency. Vertical dashed black and solid green lines mark the 3 dB and 40 dB boundaries, respectively, of the proposed CMIS channel set.

this purpose [11]. Detailed source information will allow the accuracy of forecasts of CISR observations from knowledge of source properties to be evaluated. Initial sources that appear to be easily identifiable for this purpose include two TDWR Doppler-Weather Radar systems located near the DFW airport; these systems are pulsed radars operating between 5600 and 5650 MHz, and appear to have been captured in the CISR dataset. The high time resolution "capture" mode data of CISR (not discussed here) can also help to classify the sources of observed. Initial source classification from capture mode data observed in the AASI campaign (Oct 2004) is described in [12].

6 CISR observations in more rural Texas

A PSR antenna rotation from 18:10:15 to 18:10:55 was selected as a representative dataset in the lower source density region represented in Figure 6. The aircraft location during these observations can be discerned in Figure 4 by noting the the tick marks on the flight path occur every 10 minutes. Figure 14 is a plot of the PSR main channel brightnesses versus time. Though the RFI observed is less dramatic than that in the DFW scan, and brightnesses remain within the range 300 to 350 K for all four channels throughout the scan, obvious RFI is still observed in Channels 1 and 2. The smaller variations observed (on the order of 5-10 K or less) in Channels 3 and 4 are difficult to classify as low-level RFI or as natural geophysical variations. For this scan, the PSR algorithm classifies 17.8% of pixels as containing RFI in 3 or more channels.

Figure 15 illustrates time histories of selected CISR channels in "average, APB off" mode (similar to those in Figures 11 and 12) during this portion of the flight. Channels omitted from this Figure again did not contain obvious RFI on the scales of the plots illustrated.

Though the number of sources apparent in Figure 15 is certainly reduced compared to the DFW overflight, significant RFI corruption is nevertheless observed. Broadband sources on the order of 20-30 MHz in bandwidth occur in the region 6150-6300 MHz, along with a source of approximately 10 MHz bandwidth near 6690 MHz.

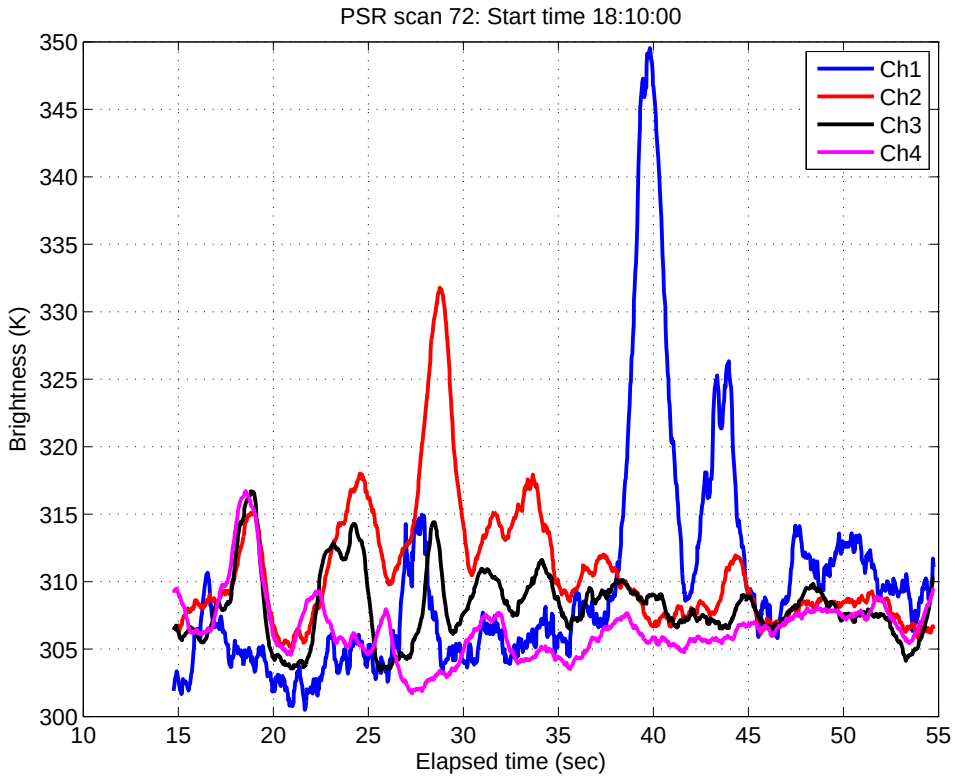

Figure 14: Vertically polarized brightnesses versus time for four PSR main channels during a portion of the flight over more rural Texas

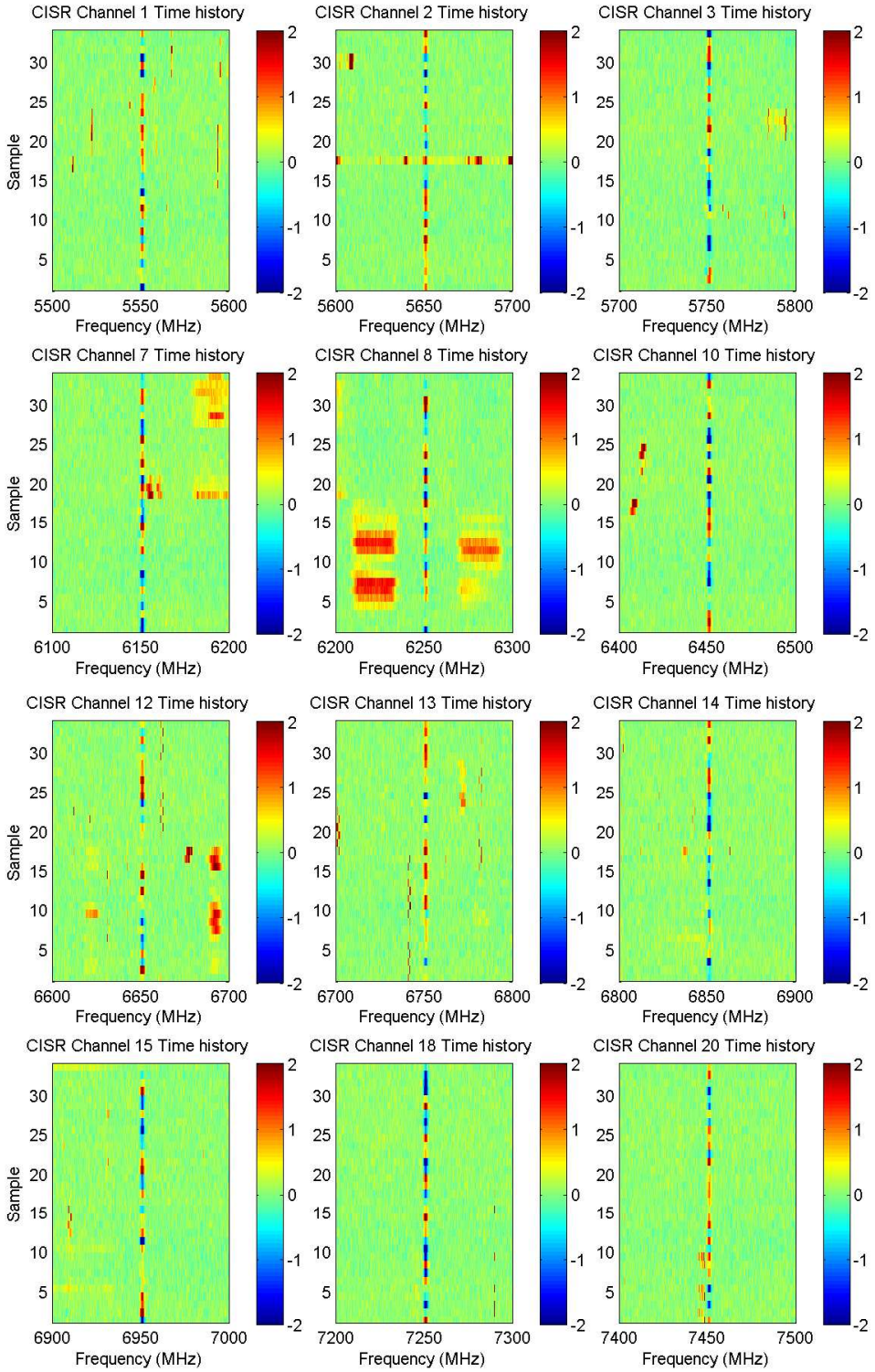

Figure 15: Time histories of selected CISR normalized spectra for portion of flight shown in Figure 14

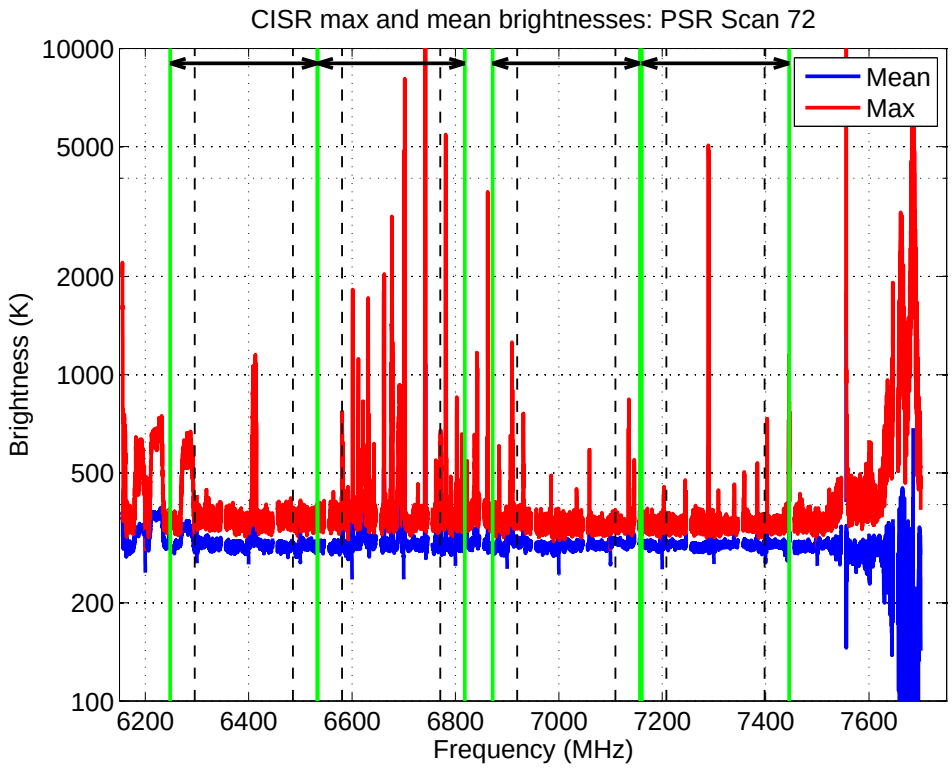

Figure 16: Mean and maximum CISR brightnesses observed in Figure 15 versus frequency. Vertical dashed black and solid green lines mark the 3 dB and 40 dB boundaries, respectively, of the proposed CMIS channel set.

Numerous narrowband sources are observed throughout the frequency range of interest; it is these narrowband sources that may contribute low-level RFI to PSR main channels 3 and 4.

The mean and maximum calibrated brightness plot for this scan is provided in Figure 16. The results shown highlight the fact that the narrowband sources included in Figure 15 do contain large brightnesses; the small bandwidth of these sources can make determination of their relative amplitudes in the plots of Figure 15 difficult. The large number of apparent sources from 6.6-7.0 GHz is consistent with Figure 15, as well as the presence of wider bandwidth sources from 6.1-6.3 GHz. RFI contributions are observed within all four of the proposed CMIS channels.

Further analysis of this dataset will be reported in a future document; the focus of these analyses will be on using CISR observations to detect and remove narrowband RFI source contributions. Such removal should be possible in this case due to the

predominance of narrowband RFI sources in these channels, combined with CISR's high spectral resolution.

7 CISR observations over the Gulf of Mexico

A PSR antenna rotation from 18:52:37 to 18:53:17 was selected as a representative dataset over the Gulf of Mexico. This portion of the flight remains in a near coastal region, so that reception of land-based RFI sources (at least 20-40 km away) remains possible.

Figure 17 is a plot of the PSR main channel brightnesses versus time. Again the dramatically large PSR main channel brightnesses observed in the DFW scan are absent, and all brightnesses remain within the range 165 to 205 K. However obvious evidence of RFI is observed in all four channels, and again, some possibility of low-level RFI remains. The lower mean brightnesses in this scan overall are consistent with observation of a sea scene. For this scan, the PSR algorithm classifies 13.25% of pixels as containing RFI in 3 or more channels.

Figure 18 illustrates time histories of selected CISR channels in "average, APB off" mode during this portion of the flight. Channels omitted from this Figure again did not contain obvious RFI on the scales of the plots illustrated. Figure 18 contains a reduced level of RFI compared to both the previous PSR scans, but both broad-band (near 6125 MHz) and numerous narrowband sources still remain. Again these narrowband sources are of particular interest for further examination to determine their production of low-level RFI in PSR main channels 3 and 4.

Mean and maximum calibrated brightnesses in Figure 19 clearly show that the narrowband sources observed produce large brightnesses (exceeding 5000 K in some cases). For this scan, proposed CMIS channel 1 appears to be the most free from contamination, while narrowband source contamination is observed in all remaining CMIS channels.

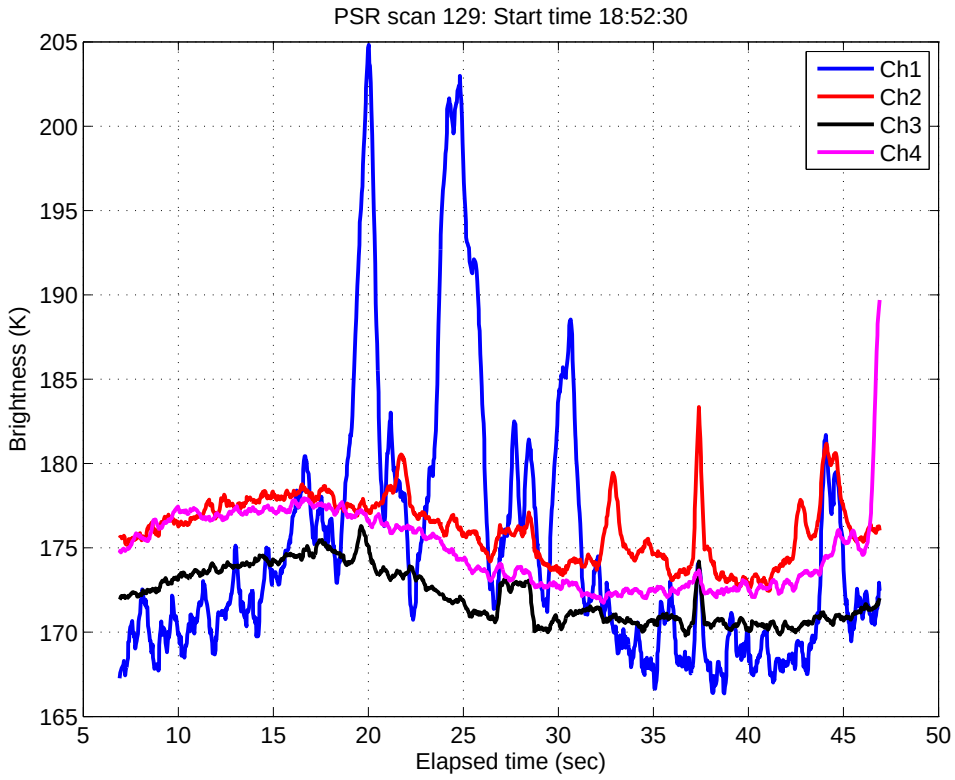

Figure 17: Vertically polarized brightnesses versus time for four PSR main channels during a portion of the flight over the Gulf of Mexico

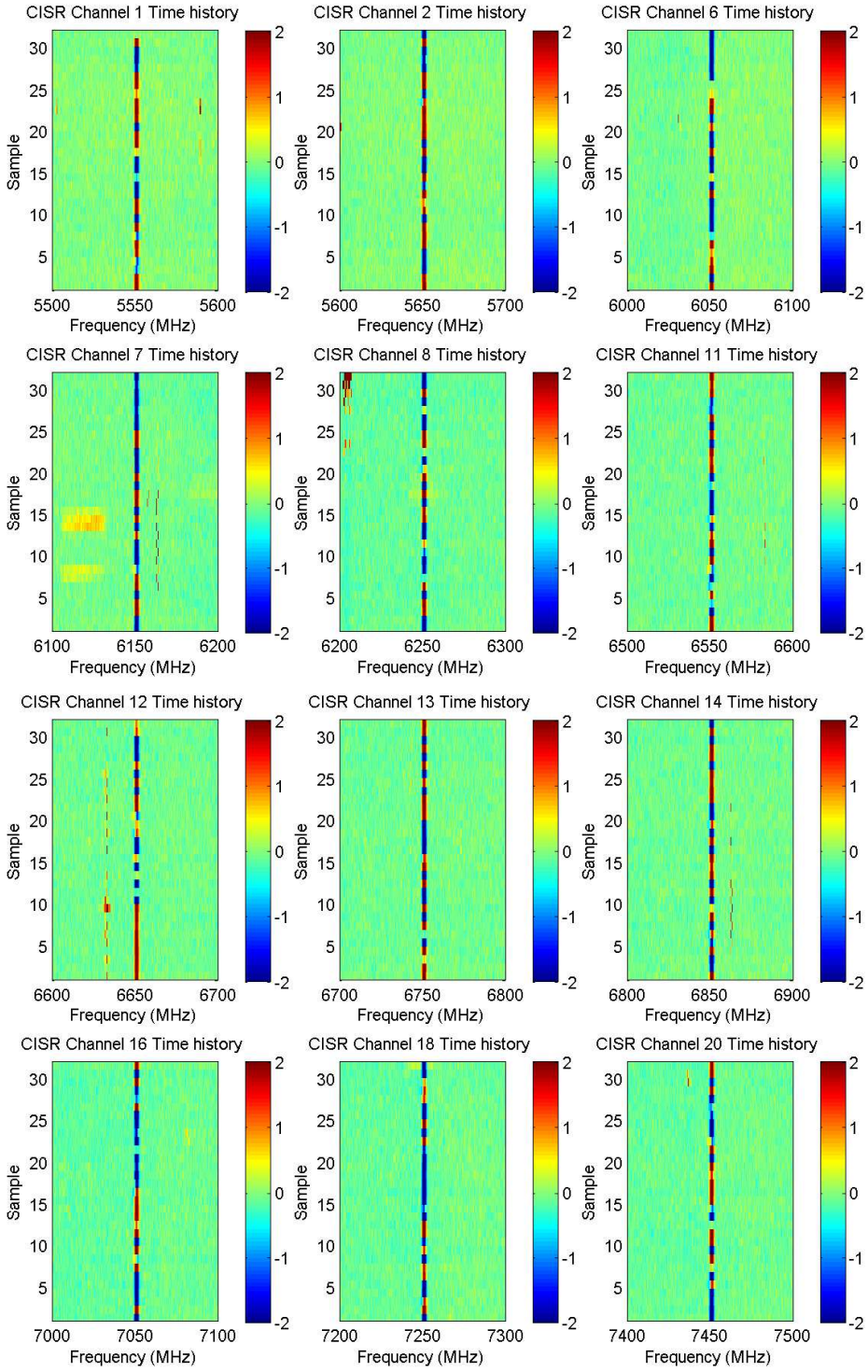

Figure 18: Time histories of selected CISR normalized spectra for portion of flight shown in Figure 17

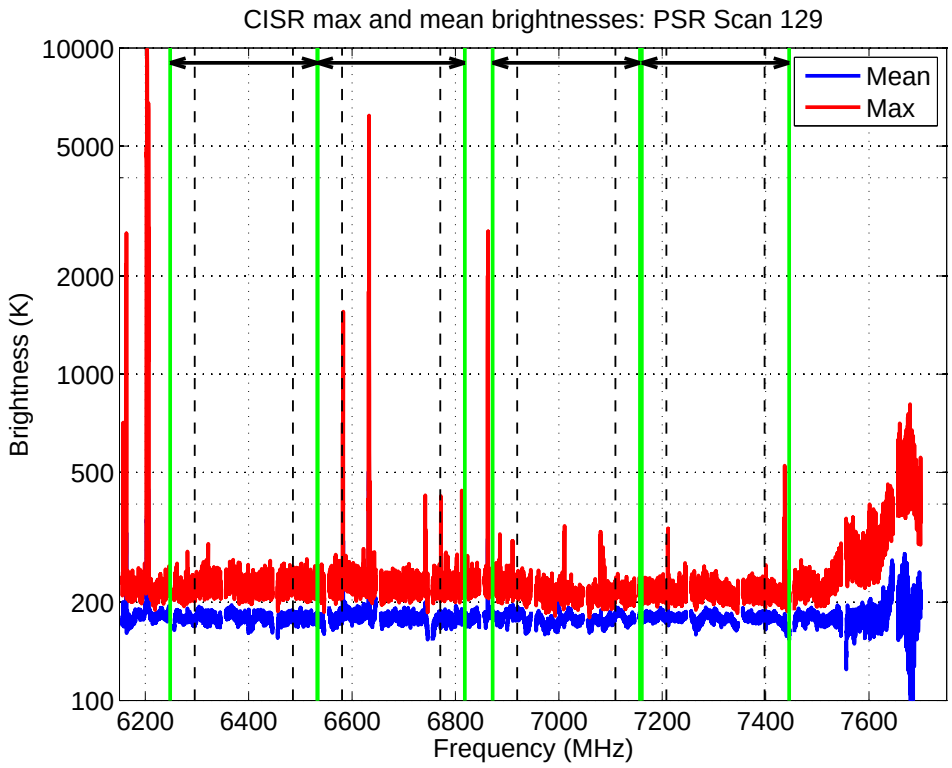

Figure 19: Mean and maximum CISR brightnesses observed in Figure 18 versus frequency. Vertical dashed black and solid green lines mark the 3 dB and 40 dB boundaries, respectively, of the proposed CMIS channel set.

8 Summary and Discussion

An initial examination of PSR and CISR data obtained from the August 25th, 2005 test flight on board the WB-57 aircraft has been provided. The approximately 125 minutes of joint data contains observations of a variety of scenes, including strong and weak RFI environments. The data clearly show the possibility of significant corruption of measured brightnesses for the proposed CMIS channels as well as other frequencies throughout C-band, with the higher frequencies typically observing less but still appreciable corruption.

Additional analyses are in progress to perform RFI source mitigation with the CISR dataset, as well as to perform assessments of the degree to which the PSR four sub-band algorithm removes low-level RFI. Further simulations of sub-band RFI mitigation with the proposed CMIS channels are also planned. Identification of sources and matchups with database information are also possible so that methods for forecasting RFI from database information can be investigated. Finally, cross-comparison of the CISR dataset with observations from the University of Michigan's C-band Agile Digital Detector (CADD) system will be performed in order to assess the effectiveness of CADD's higher-order-moment RFI detection strategies.

CISR operated without difficulty in this campaign, and is prepared for further deployments. Such deployments are recommended in order to allow RFI observations in a larger variety of RFI environments, as well as to allow continued evaluation of RFI detection and mitigation strategies. CISR observations can also be utilized for CMIS channel planning purposes to help to identify portions of the C-band spectrum that may yield reduced RFI.

References

[1] J. T. Johnson, A. J. Gasiewski, B. Guner, G. A. Hampson, S. W. Ellingson, R. Krishnamachari, N. Niamsuwan, E. McIntyre, M. Klein, and V. Leuski, "Airborne radio frequency interference studies at C-band using a digital receiver," accepted by *IEEE Trans. Geosc. Rem. Sens.,* 2006. (also available at `http://www.ece.osu.edu/~johnson/cisrpaper.zip`)

[2] Ruf, C. S., S. M. Gross, and S. Misra, "RFI detection and mitigation for microwave radiometry with an agile digital detector," *IEEE Trans. Geosc. Rem. Sens.,* vol. 44, pp. 694–706, 2006.

[3] Gasiewski, A. J., M. Klein, A. Yevgrafov, and V. Leuski, "Interference mitigation in passive microwave radiometry," *Int'l Geoscience and Remote Sensing Symposium (IGARSS 02),* conference proceedings, 2002.

[4] McIntyre, E., A. J. Gasiewski, M. Klein, V. Leuski, B. L. Weber, and V. Irisov, "Experimental results from a spectral scanning technique for passive remote sensing of soil moisture," *U. S. National Radio Science Meeting,* conference proceedings, 2006.

[5] MicroLambda Website, `http://www.microlambdawireless.com/YIG-Oscillators/EMYTOs/X-Series-SatCom.htm`.

[6] J. T. Johnson and S.W. Ellingson, "Digital Receiver with Interference Suppression for Microwave Radiometry," project website, `http://esl.eng.ohio-state.edu/~rstheory/iip/docserv.html`.

[7] J. T. Johnson, B. Guner, and N. Niamsuwan, "Observations of an ARSR system in Canton, MI with the L-band interference suppressing radiometer," project report, Dec 2005. (available at `http://esl.eng.ohio-state.edu/~rstheory/iip/lisr_jtj.pdf`)

[8] S. W. Ellingson, personal communication, Nov. 2005.

[9] Regner, M., N. Chauhan, and D. Kunkee, "NPOESS CMIS: RFI Issues and Progress," presentation available at: http://eic.ipo.noaa.gov/IPOarchive/SCI/sensors/cmis/igarss04.pdf.

[10] D. B. Kunkee, personal communication, Sept 2005.

[11] Federal Communications Commission Universal Licensing System search page, http://wireless2.fcc.gov/UlsApp/UlsSearch/searchLicense.jsp.

[12] S. W. Ellingson and K. H. Lee, "Analysis of persistent RFI signals captured using the CISR coherent sampling mode," project report, 2006. (available at http://www.ece.osu.edu/~johnson/cisr/cisr0602.pdf)